Heterogeneous nucleation and adatom detachment at one-dimensional growth of In on Si(100)-2×1

Jakub Javorský, Martin Setvín, Ivan Ošťádal,* and Pavel Sobotík
Department of Surface and Plasma Science, Charles University, V Holešovičkách 2, 180 00 Prague 8, Czech Republic

Miroslav Kotrla
Institute of Physics, Academy of Sciences of the Czech Republic, Na Slovance 2, 182 21 Prague 8, Czech Republic
(Received 29 December 2008; published 17 April 2009)

Growth of atomic indium chains—one-dimensional islands—on the Si(100)-2×1 surface was observed by scanning tunneling microscopy (STM) at room temperature and simulated by means of a kinetic Monte Carlo method. Density of indium islands and island-size distribution was obtained for various deposition rates and coverage. STM observation of growth during the deposition of indium provided information on growth kinetics and relaxation of grown layers. Important role of *C*-type defects at adsorption of metal atoms was observed. Measured growth characteristics were simulated using a microscopic model with anisotropic surface diffusion and forbidden zones along the metal chains. An analysis of experimental and simulation data shows that the detachment of indium adatoms from the chains substantially influences a growth scenario and results in monotonously decreasing chain length distribution function at low coverage. Diffusion barriers determined from the simulations correspond to almost isotropic diffusion of indium adatoms on the surface. The results are discussed with respect to data reported in earlier papers for other metals.

DOI: 10.1103/PhysRevB.79.165424 PACS number(s): 68.55.ag, 68.37.Ef, 81.15.Aa

I. INTRODUCTION

The Si(100)-2×1 surface is composed of silicon atom pairs—dimers—arranged into rows. It represents a natural template for spontaneous growing linear structures of many materials such as group III-V metals. Group III metals (Al, Ga, In, and Tl) are known to grow in one-dimensional (1D) atomic chains when deposited on the Si(100) surface.[1–4] Technique of scanning tunneling microscopy (STM) enabled the detailed study of metal layers with atomic resolution. An especially powerful tool for the investigation of growth kinetics is the STM *in vivo* technique,[5,6] which allows the direct monitoring of the layer as it grows. 1D metal chains grow perpendicularly to the underlying silicon dimer rows of the Si(100)-2×1 surface. They are composed of metal dimers (oriented parallel to the silicon dimers) sitting in the "trenches" on the silicon surface.[7] Growth of the metal chains has been explained by a surface polymerization reaction.[8] Metal chain ends act as nucleation centers. Since the sites adjacent to a chain are energetically unfavorable for adsorption (no adsorption has been observed there), the chains grow only in length. The chains are always separated by a distance of at least $2a$ (a=0.384 nm, surface unit-cell spacing). Thus, the surface is saturated by metal adatoms at a coverage of 0.5 ML (1 ML=6.78×10^{14} cm^{-2}). Some differences exist between various group III metals. While Al and Ga chains are believed to be stable at room temperature (RT),[8,9] indium atoms are known to detach from chains and reattach to other chains[10] and Tl chains were shown to be even more unstable.[4] Though a qualitative description of diffusion and growth processes for group III metals exists, the corresponding values of microscopic parameters are not known. The heights of diffusion barriers on Si(100) have not been yet determined for In and the values reported by Albao *et al.*[9] for Ga and by Brocks *et al.*[8] for Al were very different. Similar discrepancy exists for the estimation of Ga dimer pair-interaction energy; Tokar and Dreyssé[11] suggested ≈ 0.2 eV while Takeuchi's *ab initio* calculation gave ≈0.8 eV.[12] Recently Kocán *et al.*[10] reported that the detachment of indium atoms from chains is length dependent, so interactions other than nearest neighbor (NN) might play a role.

The role of surface defects present on the Si(100)-2×1 surface[13] at the metal adsorption and nucleation was reported and discussed.[10,14–16] Experimental results showed that the influence of *A*- and *B*-type defects (one and two missing dimers, respectively) can be neglected but *C*-type defects are important. The *C*-type defects, which appear on STM images as a small bright protrusion next to a dark spot in filled states and as a larger bright spot in empty states, are reported to be very reactive and act as nucleation centers.[10,14] The *C* defects were independently interpreted by Hossain *et al.*[17] and Okano and Oshiyama[18] as dissociated H_2O molecules, with the H and hydroxyl group bonded to neighboring silicon atoms of two adjacent surface dimers. The results both of experimental and theoretical study of In nucleation at the *C* defects were reported in Ref. 16. After adsorption of an In adatom at a *C* defect (exclusively on the unoccupied side of the two adjacent Si dimers), the chain begins to grow in one direction only (see Fig. 1 in Ref. 16). The chain termination at the defect is stable; the opposite "free" end is active as an adsorption site for adatoms.

Albao *et al.*[9] reported growth characteristics for Ga on Si(100) at RT. An unconventional monotonously decreasing scaled island (chain) size distribution function obtained for low coverage was explained by an irreversible growth model and kinetic Monte Carlo (KMC) simulations. The simulations resulted in the monotonous size distribution only if the highly anisotropic surface diffusion of Ga adatoms was introduced, otherwise a monomodal form of the distribution

function was obtained. The presence of *C* defects included later[14,15] did not change the results significantly; similar growth characteristics at RT we reported for indium.[19] The chain length distributions obtained for various coverages are monotonously decreasing and obey a scaling relation. Most of In chains (60–90 %) in observed layers were on at least one end terminated by a *C*-type defect. In the *in vivo* experiments, the percentage was higher (90–100 %) (due to low deposition rates of In during the *in vivo* measurements). Density of indium chains and average chain length depends on *C*-defect concentration. Another phenomenon (observed at higher coverage) is that indium atoms are able to migrate throughout sites adjacent to an indium chain even though no adsorption is observed (such an effect seems to be negligible at low coverage).

In this paper, we use STM data and KMC simulations for detail studying indium growth on the reconstructed surface Si(100)-2×1. A growth model, which includes the presence of *C* defects and a process of atom detachment from indium chains, is used for studying a role of *C* defects at metal chain nucleation, determination of diffusion barriers, and investigation of the relation between growth processes and a form of chain length distribution function. Processes and parameters included in the growth model are discussed with respect to experimental data obtained by means of STM.

Performed experiments are characterized in Sec. II, consequently experimental results are presented in Sec. III, a simulation model is described in Sec. IV, results of simulations are compared with the experimental data and discussed in Sec. V, and formulas for the calculation of deviations between experimental and simulated growth characteristics are given in the Appendix. Finally, Sec. VI contains our conclusions.

II. EXPERIMENTAL

All experiments were carried out at room temperature in a noncommercial UHV STM system with base pressure $<3\times10^{-9}$ Pa. Si(100) samples were cut from an *n*-type Sb-doped silicon wafer with resistivity $\leq0.014\ \Omega$ cm. To obtain the 2×1 reconstruction, samples were flashed several times for ≈20 s to ≈1200 °C. Indium was deposited from tungsten wire evaporators either before or during imaging the surface by means of STM. In the latter case (experiment *in vivo*), a miniature evaporator was in a distance of 4 cm from the sample and a beam of In atoms was determined by means of two apertures with a diameter of 1 mm. Incidental angle of the beam was 30°. The apex shape of a tungsten electrochemically etched tip enabled deposition "under" the STM tip onto the scanned area. The thermal drift during deposition was compensated by the STM control unit. The *in vivo* measurements provided continuous STM imaging of the investigated surface area before and during the deposition at a rate of 1 image/min. At standard *in situ* measurements, the indium layers were observed 0.5–4 h after deposition. We used a tip voltage of +2 V and tunneling current 0.3 nA; the values at which tip influence on the detachment of indium adatoms from the chains is minimized as we proved earlier.[10]

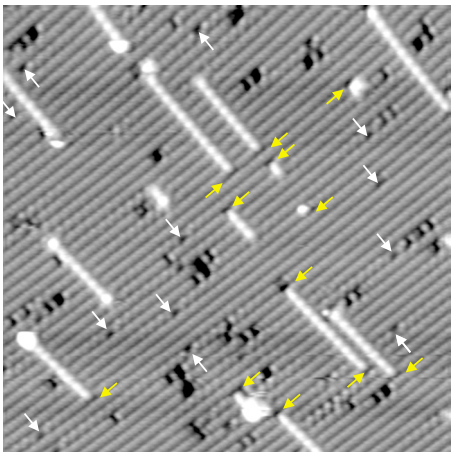

FIG. 1. (Color online) Filled state STM image of indium 1D chains grown at room temperature on the surface Si(100)-2×1. The bright spots at ends of some chains indicate termination by a single indium atom (Refs. 10 and 16); stable terminations at *C* defects are marked by the arrows perpendicular to chains. Unoccupied *C* defects are marked by the arrows parallel with chains; the arrows are directed from the side of possible chain growing. Coverage 0.044 ML, *in situ* measurements 2 h after deposition; image size 30×30 nm^2.

III. EXPERIMENTAL RESULTS

An example of indium chains grown on the Si(100) surface at low coverage is shown in Fig. 1. Length of the chains can be easily determined with atomic precision from filled states images where the "free" terminations of chains containing an odd number of atoms appear much brighter than in case of even number.[10,14] Chain terminations at *C* defects and unoccupied *C* defects are marked by arrows. Concentration of the *C* defects increases during deposition at *in vivo* experiments (probably due to thermal desorption of residual water molecules from heated parts near the evaporation source in a relatively small distance from the sample). The increase was found linear and corresponds to a deposition rate of 4×10^{-6} ML/s. The deposition rate of *C* defects at *in situ* experiments was negligible (due to a large distance of the evaporation source and better screening of the sample) and the initial concentration of the *C* defects can be considered as unchanged.

Since the atomic structure of In chains is well known,[7,10,16] we focused on statistical characteristics of the chains. Obtained data are summarized in Table I. The data were acquired from images of the size of 30×30 nm^2 or 40×40 nm^2. The image areas are large enough (30 nm corresponds to a ~100-atoms long chain) and the resolution is sufficient to discern the number of atoms in the chain. Data were collected only from terraces much wider than an average chain length to exclude the influence of step edges on the chain growth. Statistical characteristics were evaluated for both types of growth experiments (*in vivo* and *in situ*).

Length of the grown indium chains evolves in time due to the attachment/detachment of single atoms to/from the "free" ends. Figure 2 contains the dependence of an average chain length on coverage obtained from two *in vivo* measurements

TABLE I. Measured statistical characteristics of In chains for various coverages and deposition rates. N is total number of investigated chains and $\langle s \rangle$ is the average chain length. Numbers of chains terminated on C defects and C defects occupied by indium chains are normalized with respect to total numbers of chains and C defects, respectively.

Coverage (ML)	Deposition rate (ML/s)	$\langle s \rangle$ all chains	$\langle s \rangle$ chains with free ends	$\langle s \rangle$ chains on C defects	Chains terminated on C defects	C defects occupied by chains	C defects coverage (ML)	N
0.01	0.03	2.78	2.87	2.77	0.90	0.14	0.014	303
0.04	0.0035	4.19	3.48	4.63	0.61	0.74	0.008	1098
0.05	0.01	4.92	6.00	4.57	0.75	0.58	0.013	154
0.08	0.002	6.64	5.14	6.95	0.83	0.93	0.011	548
0.09	0.0045	8.20	6.71	8.69	0.75	0.68	0.013	69
0.15	0.003	18.29	19.29	17.60	0.59	0.94	0.005	207

with deposition rates 6×10^{-5} and 1×10^{-4} ML/s and a number of *in situ* measurements for various deposition rates (from 2×10^{-3} to 3×10^{-2} ML/s) and coverages (0.01–0.15 ML). The average length of chains is smaller in the case of *in vivo* experiments because of the higher concentration of C defects and from the coverage 0.25 ML (which corresponds to the occupation of a half of all possible adsorption sites on the surface) almost does not increase.

Figure 3 shows histograms of chain length distributions for two different coverages obtained from *in situ* experiments. The data were averaged over STM images taken after the deposition from various surface areas. The chains nucleated on C defects are distinguished from the "free" chains (without termination on a C defect). The histograms contain also single In atoms adsorbed and trapped on C defects. They represent stable objects with a role of nucleation centers. Their presence in the histograms allows better understanding of the growth, but we consider only chains with length $s \geq 2$ as parts of the investigated "island population." The histograms are decreasing for $s>1$ and the same tendency was observed for the other prepared layers with low coverages $\leq$0.15 ML. The monotonously decreasing chain length distributions obtained for the growth of indium at RT represent a remarkable quality. It can be seen that histograms contain some features related to details of the chain growth—a small excess of chains containing even number of atoms which corresponds to the higher stability of such chains experimentally observed[10] and calculated[16] before.

The chain length distributions exhibit scaling:[20,21] the function $N_s\langle s \rangle^2/\Theta$ scales with $s/\langle s \rangle$, where N_s is density per site of chains of the length s, $\langle s \rangle$ is the average chain length, and Θ is the coverage. The upper panel (a) of Fig. 4 shows the scaled distribution functions corresponding to the various delay between the end of deposition and STM measurements at the *in situ* experiments. Only chains with $s \geq 2$ were included. All the data were fitted by an exponential function. Due to statistical fluctuations in the data, it is difficult to distinguish reliably an effect of the postdeposition relaxation. The postdeposition relaxation can be expected because of the process of detachment, which introduces a feature of "reversibility" into a growth mechanism. We will discuss the "reversibility" and postdeposition relaxation later in Sec. V.

The scaled distributions obtained from the images recorded at *in vivo* measurements are in the bottom diagram (b) in Fig. 4. The data suffer from the limited size of the investigated surface area and relatively small number of observed metal chains. Values for a particular distribution cor-

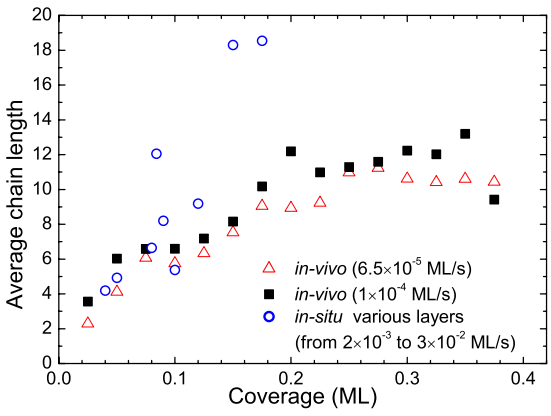

FIG. 2. (Color online) Dependence of the average chain length on coverage obtained from STM experiments. The average length of In chains increases with coverage and saturates at a coverage of 0.25 ML for the *in vivo* data. The dependence increases faster for the layers prepared at *in situ* experiments due to smaller and constant concentration of C defects. The effective deposition rate for C defects was 4×10^{-6} ML/s during the *in vivo* measurements.

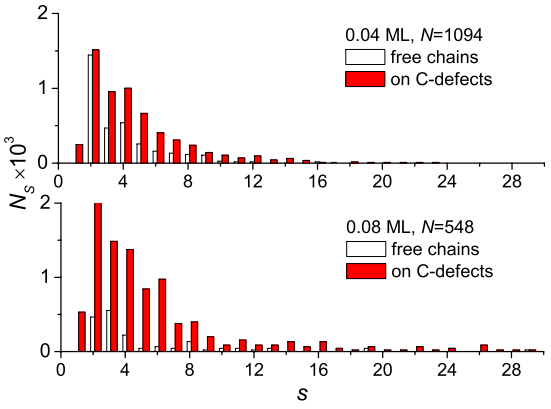

FIG. 3. (Color online) Histograms of the chain length distribution obtained for two indium layers with coverage of 0.04 and 0.08 ML deposited at a deposition rate of $\approx$0.004 and $\approx$0.002 ML/s, respectively (*in situ* experiments). For comparison, histograms contain single indium atoms trapped on C defects. N represents a number of investigated chains.

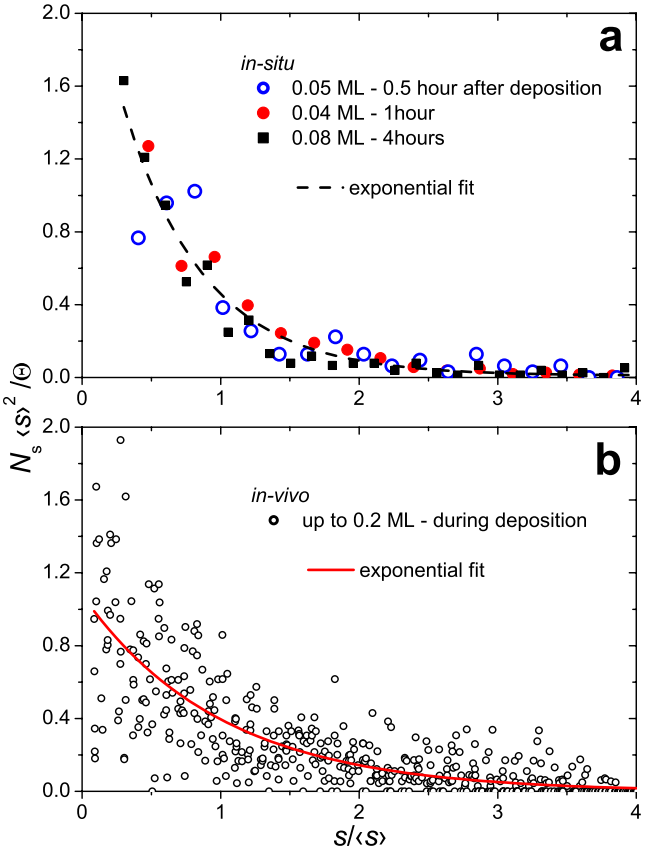

FIG. 4. (Color online) Scaled island-size distribution functions obtained from experimental data. (a) Results from three *in situ* measurements performed at various moments after deposition. (b) Data obtained during deposition (*in vivo*) composed from a set of 15 histograms covering equally the whole deposition. The data were fitted by exponential functions.

responding to a chosen moment (coverage) of the growth were averaged from a set of three subsequent STM images around that moment. The whole recorded sequence of images taken during the growth up to 0.2 ML at a deposition rate of 0.000 1 ML/s (estimated from the images) is represented "equidistantly" by the 15 distributions. The rather scattered data exhibit monotonous character and can be approximated by an exponential function.

IV. SIMULATION MODEL

We developed a physical atomistic model for the submonolayer growth of indium on Si(100). Similarly as in the model used by Albao *et al.*[9] to describe growth of gallium layers at low coverage, we consider the anisotropic diffusion of the metal adatoms on the 2×1 reconstructed surface. However, we took into account experimental results obtained for In and included new features: the presence of *C* defects acting as nucleation centers on the surface and detachment of single atoms from chains. The mechanism of detachment introduces into the growth model a possibility of "reversible" behavior ("reversible" does not mean here "equilibrium," due to existing flux of deposited atoms). Approaching an equilibrium state depends on growth conditions and it competes with kinetics which controls growth entirely in case of an irreversible model used for gallium.

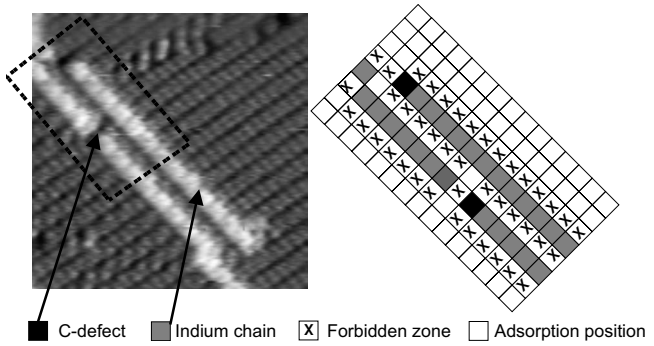

FIG. 5. Left: filled state image of indium chains. The two neighboring chains are separated by a distance of one lattice unit. Dark spots at the ends of chains are *C* defects. Right: alignment of the model to Si(100) substrate. The black square represents the "reactive site" at the *C*-defect position, gray squares represent adsorption sites occupied by indium adatoms, empty squares represent unoccupied adsorption sites, and crossed squares represent "forbidden zones" energetically unfavorable adsorption sites.

The model for In deals with four types of objects on the surface (see Fig. 5). (1) Free In adatoms: indium atoms perform thermally activated hopping on the surface represented by a square lattice (see Fig. 5). The hopping is anisotropic (parallel and perpendicular to indium chains) described by rates $h_{\parallel,\perp}=\nu\exp[-E_{\parallel,\perp}/(k_BT)]$, where the attempt frequency was set as $\nu=10^{13}$ s^{-1}, the activation energies (diffusion barriers) $E_{\parallel}$, $E_{\perp}$ are simulation parameters, k_B is the Boltzmann constant, and T is the temperature.

(2) Forbidden zones: surface sites not accessible for hopping adatoms. The forbidden zones were introduced, similarly as in Ref. 9, to simulate the 1D growth, minimum separation observed between two adjacent chains, and the fact that no chain nucleates at a "nonreactive" side of a *C* defect.

(3) *C*-type defects—dissociated H_2O molecules—rest on top of dimer rows. STM observations show that one side of the *C* defect acts as a nucleation center while no adatom adsorption has been observed on the opposite "dark" side (on filled state STM image) of the defect. Thus, *C*-type defects are represented by a single forbidden site and an adjacent "reactive" site.

(4) Indium chains—orientated perpendicularly to the Si dimer rows—are composed of two or more In atoms. Similarly as in the model used by Albao *et al.*,[9] the arrangement of atoms in chains into dimers is not taken into account.

There are three main processes in our model. (A) Deposition: adatoms and *C* defects are deposited randomly. If a defect or an adatom is deposited on an already occupied position or (in case of In atoms) into a forbidden zone, the nearest free position is looked up in the direction of dimer rows. Deposition flux and time were set the same as in the particular experiments (indium flux 10^{-2}–10^{-5} ML/s; *C* defect flux 4×10^{-6} ML/s, for "*in vivo*" only) and corresponding simulations were performed for all STM experiments. Orientation of a deposited *C* defect (reactive site) was chosen randomly. As the *C* defects change their state only very rarely,[16,22] the orientation is fixed during the whole

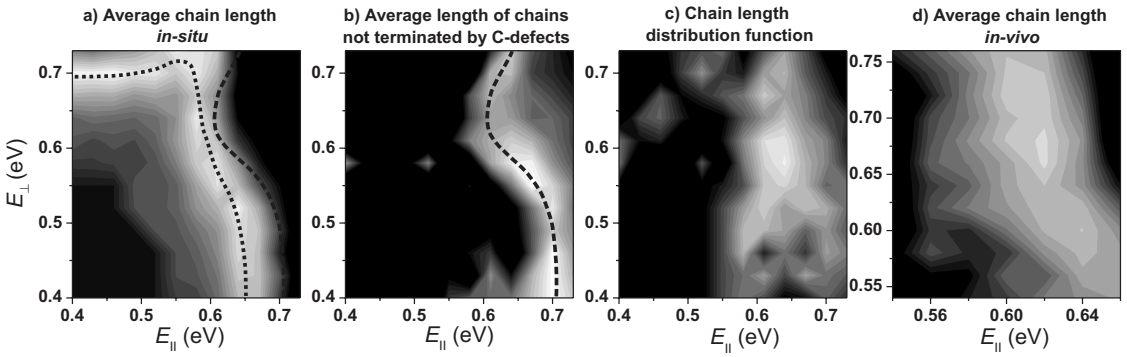

FIG. 6. Maps showing the deviation between the measured and simulated characteristics of indium chains as a function of diffusion barriers parallel and perpendicular to In chains. White areas indicate the best agreement; black areas the worst. Dotted line connects local minima in panel (a), dashed line in panel (b). Dashed line from panel (b) is also shown in panel (a) for comparison. The best combination of energies $E_{\|}=0.62\pm0.03$ eV and $E_{\perp}=0.61\pm0.07$ eV obtained from (a) and (b) indicates almost isotropic diffusion and agrees within errors with minima on panels (c) and (d) (see text for details). Energy barrier for atom detachment was 0.82 eV. Only the detachment parallel to indium chains was allowed in these simulations.

simulation (it differs from Ref. 15, where the orientation was determined each time when an adatom tried to hop next to the defect).

(B) Surface migration (hopping): single indium atoms deposited on the surface perform random hops among adsorption sites. Jumps to forbidden zones and on top of other atoms are prohibited. An atom is trapped when hops onto a *C* defect reactive site. If an atom hops on a site next to another atom in the direction parallel to In chains (perpendicular to the dimer rows), a new indium chain nucleates or an existing one grows. The hopping rates $h_{\|,\perp}$ in directions parallel or perpendicular to the indium chains are given by the simulation parameters $E_{\|}$ and $E_{\perp}$ (diffusion barriers parallel and perpendicular to indium chains).

(C) Detachment: an indium atom can detach from a chain end, not terminated by a *C* defect, by jumping off either in perpendicular or in parallel direction to the chain. According to our best knowledge, there are neither experimental nor theoretical data available to characterize the detachment direction in the studied (or similar) system on the atomic level. The process of the detachment is thermally activated and can be described by two parameters: $E_{\mathrm{det}\|}$ and $E_{\mathrm{det}\perp}$ (energy barriers for the detachment in the parallel and in perpendicular directions). Our previous measurements[10] and theoretical calculations[16] show that the energy for detachment depends on length and termination of an In chain by a single atom or dimer. The detachment from a chain containing an odd number of atoms is easier than in the case of even number. For simplicity, the model contains only one parameter—the value of a mean energy barrier for detachment (0.82 eV) derived from experimental data reported in Ref. 10. As we know only the total rate of detachment without any details, simulations were performed for detachment either in the parallel or in the perpendicular direction. Two-atomic chains (dimers) on *C* defects are considered as stable objects which cannot decay (both experiment and theoretical calculations[16] confirmed their high stability).

The simulation proceeds as follows. *C* defects are randomly deposited on the surface with initial concentration. Then indium atoms are randomly deposited (together with additional *C* defects according to a simulated experiment). For details of an employed method of KMC simulations, see Ref. 23. After the deposition stops, the layer is allowed to relax for the same time as in the corresponding experiment. The Si(100)-2×1 surface is represented by a square matrix of adsorption sites, each capable of holding a single indium atom. We used a matrix size between 100×100 and 500×500 lattice units, each simulation was repeated at least nine times and the obtained data were averaged. The values of the matrix size were chosen so as the mean average error of simulated data was 2–3 times smaller than that of measured data (the size of statistical arrays varied for different values of coverage). The boundary conditions were periodic.

V. RESULTS OF SIMULATIONS AND DISCUSSION

A. Diffusion barriers

The *in situ* and *in vivo* experiments were simulated for various combinations of diffusion barriers $E_{\|}$ and $E_{\perp}$. Comparison of experimental and simulated growth characteristics (average chain length, dependence of average chain length on coverage, and scaled chain length distribution) was used for the estimation of a combination of barriers which provides the best agreement; the lowest deviation calculated as presented in the Appendix.

Figure 6 contains diagrams with the dependence of the calculated deviations on the simulation parameters $E_{\|}$ and $E_{\perp}$ for the chosen growth characteristics. The grayscale represents accuracy of the match for a given combination of parameters with white for the most precise match. The plots (a) and (b) demonstrate fitting the *in situ* measurement for a layer with coverage 0.08 ML. In plot (a) the dotted black line shows the combinations of activation energies which provide the best match between the measured and simulated average length of indium chains; the dashed line in plot (b) shows the best agreement for the average length only of those chains which are not terminated by *C* defects at any of ends. The relatively small "subpopulation" of these chains behaves in a different way so the two plots together were used to deter-

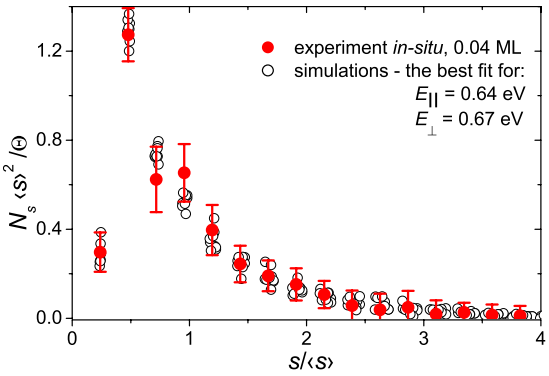

FIG. 7. (Color online) Experimental and simulated scaled chain length distribution functions for a relaxed layer at coverage 0.04 ML (*in situ* experiment). Results of various simulation experiments for the same parameters $E_{\parallel}$ and $E_{\perp}$ are plotted. Data representing single indium atoms trapped on *C* defects are plotted as well (on the very left side).

mine the best combination of energies: $E_{\parallel}=0.62\pm0.03$ eV and $E_{\perp}=0.61\pm0.07$ eV. The values are consistent (within the errors) with the optimum combination of energies obtained from fitting the average chain length dependence on coverage from *in vivo* measurements [see Fig. 6(d)].

Further we simulated experimentally obtained scaled chain length distributions. Fitting was performed for the two *in situ* measurements which provided the largest data sets (0.04 and 0.08 ML coverage) and for the *in vivo* measurements. As an example of the analyzed data, we show in Fig. 7 simulations of experimental data for a distribution function. The simulations were performed for the energies $E_{\parallel}=0.64$ eV and $E_{\perp}=0.67$ eV and correspond to a layer with coverage 0.04 ML (see Table II). The plot, in addition to points representing the whole chain population for $s\geq2$, contains the points corresponding to single indium atoms trapped on *C* defects. The deviation used for the final fitting was a sum of D_{iii} values calculated using the relation (4) for the three chosen measurements [see Fig. 6(c)]. Comparison of experimental and simulated data resulted also in almost isotropic diffusion of In on Si(100) with activation energies very close to the values obtained by the fitting represented by the diagrams (a), (b), and (d).

We studied how the best fit of growth characteristics is affected by a change in the value of the detachment energy.

TABLE II. Activation energies for In adatom diffusion parallel and perpendicular to In chains for two directions of detachment. Values were obtained by comparing data from two *in situ* and one *in vivo* experiments and simulations for two models considering different atom detachment from chains.

	Parallel detachment		Perpendicular detachment	
	$E_{\parallel}$ (eV)	$E_{\perp}$ (eV)	$E_{\parallel}$ (eV)	$E_{\perp}$ (eV)
0.04 ML	0.64 ± 0.03	0.62 ± 0.07	0.64 ± 0.03	0.67 ± 0.07
0.08 ML	40.62 ± 0.03	0.61 ± 0.07	0.61 ± 0.03	0.64 ± 0.07
In vivo	0.60 ± 0.10	0.65 ± 0.05	0.65 ± 0.10	0.65 ± 0.05

We performed additional simulations using values of the detachment energy from the interval ±0.04 eV around the experimental value 0.82 eV which we used in our KMC simulations. The simulations showed that increasing or decreasing the detachment energy results in increasing or decreasing the diffusion barriers, respectively. The change is practically the same for both the barriers $(E_{\parallel},E_{\perp})$ and equals the change in the detachment energy. If diffusion barriers remain unchanged, the increase in the detachment energy results in lowering concentration of free chains (not terminated on *C* defects) and the average chain length slightly increases; decreasing the detachment energy increases the number in the free chains and the corresponding decrease in the average chain length is observed.

In addition, we investigated how the direction of the detachment of atoms from chains affects values of the estimated diffusion barriers. We found that the direction of detachment does not affect results significantly when the diffusion is nearly isotropic; it plays an important role only in the case of very anisotropic diffusion. Table II shows the energy barriers obtained from simulations of different experiments fitted using both the parallel and perpendicular directions of detachment. Any combination of the energies outside the range given by included errors results in a double deviation (compared to the best fit) between experimental and simulated data. The activation energies obtained for the parallel detachment are slightly lower than for the perpendicular one.

The diffusion barriers for indium determined from KMC simulations (see Table II) correspond to almost isotropic diffusion. It is in contrast to Albao's *et al.* anisotropic results ($E_{\parallel}=0.40$ eV; $E_{\perp}=0.81$ eV). The values obtained theoretically for Al by Brocks *et al.*[8] are anisotropic as well ($E_{\parallel}=0.1$ eV; $E_{\perp}=0.3$ eV) but much lower.

B. Scaled chain length distribution function

It follows from the nucleation theory[20,24] that during the submonolayer growth, the density (per site) N_s of islands composed of *s* atoms fulfils the scaling form,

$$N_s \approx \Theta \frac{f(s/\langle s \rangle)}{\langle s \rangle^2}, \tag{1}$$

where Θ is the coverage and $\Theta/\langle s \rangle$ represents the mean island-size density. The function $f(x)$, $x=s/\langle s \rangle$ is the scaled island-size distribution function. The relation (1) was confirmed by simulations using different models of irreversible two-dimensional (2D) aggregation and from STM experiments. In most cases, the shape of the scaled distribution function is monomodal, with a peak for $x=1$. A monomodal function was observed both for homogeneous and heterogeneous nucleations. The scaling for the passage from irreversible to reversible aggregation was examined theoretically in Ref. 21. The unconventional shape of the scaled distribution function, monotonously decreasing, observed for 1D growth of Ga on Si(100) by Albao *et al.*[9] (and explained by means of KMC simulations using strongly anisotropic surface diffusion) was theoretically investigated by Tokar and Dreyssé.[11] They showed that for equilibrium growth and a model with

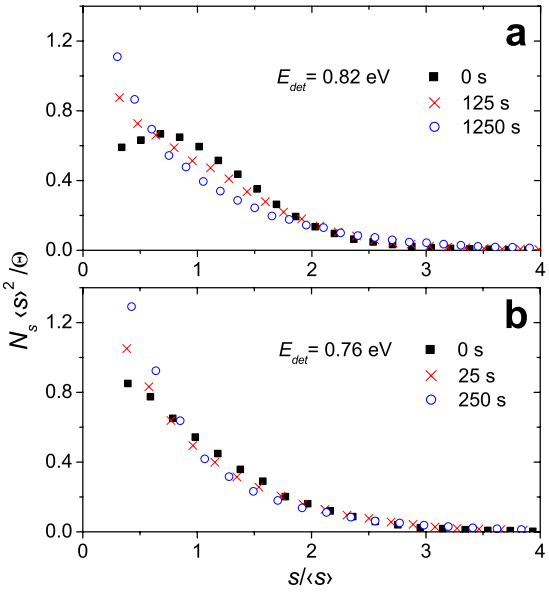

FIG. 8. (Color online) Postdeposition relaxation of a simulated scaled distribution functions for two detachment barriers (a) 0.82 eV and (b) 0.76 eV. The transition to the monotonically decreasing function corresponding to an equilibrium state is visible. The simulation corresponds to a layer with coverage 0.08 ML deposited at rate 0.002 ML/s.

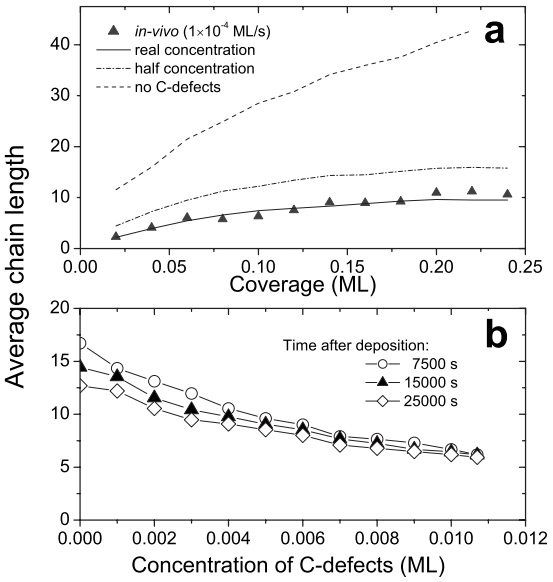

FIG. 9. (a) Dependence of the average chain length on coverage simulated for various concentrations of C defects. Triangles represent data from the corresponding *in vivo* experiment. (b) Average chain length is controlled by the concentration of C defects. Note also the relaxation of the average chain length during time. $E_{\parallel}=0.62$ eV and $E_{\perp}=0.58$ eV, $E_{\mathrm{det}}=0.82$ eV.

atomic interactions restricted to only nearest neighbors, the scaled distribution function is exponentially decreasing. Here we obtained for 1D submonolayer growth of In similar monotonously decreasing chain length distribution functions (Figs. 4 and 7).

If we consider the homogeneous nucleation with the detachment only and the C defects are excluded from our model, the simulated distribution function remains monotonously decreasing. On the other side, excluding the process of detachment (irreversible model) results in a conventional monomodal distribution function independently of presence of the C defects in the model. For the irreversible model, the monotonous distribution can be simulated only when the strong diffusion anisotropy is introduced, similarly as reported by Albao *et al.*[9] We conclude that the monotonous form of the chain length distribution function obtained for indium layers with low coverage ($\leq$0.15 ML) at RT and used deposition rates can be explained by the process of atom detachment from indium chains during the growth.

C. Postdeposition relaxation

Further we used our reversible growth model for exploring postdeposition relaxation indicated by experimental data obtained from STM measurements at various time after deposition (see Fig. 4). We simulated the growth using the diffusion barriers determined and deposition rate 0.002 ML/s for two different values of the detachment barrier. The time evolution of the distribution functions obtained for various time after deposition is in Figs. 8(a) and 8(b). If the detachment rate is small enough with respect to the deposition rate (a high-energy barrier for detachment), the distribution function is monomodal just after the deposition and relaxes into a monotonous one [Fig. 8(a)]. If the detachment rate increases, the distribution function changes from the monomodal to monotonous form even during the growth [see Fig. 8(b)]. The simulation shows that the observed system reaches an equilibrium state after ~6 h (estimation for the used experimentally determined barrier $E_{\mathrm{det}}=0.82$ eV), though the most dramatic change occurs during the first 10 min after the deposition.

D. Influence of C defects

The time constant for the detachment of an In atom from an adsorption site at a C defect is $\approx$100 times bigger than for the detachment from In chains, making the C defects practically perfect diffusion traps.[10] To describe a role of C defects at heterogeneous nucleation and submonolayer growth of In quantitatively, we simulated growth using the same parameters as for a real experiment, only the concentration of the C defects was changed. Figure 9(a) shows the dependence of the average chain length on coverage obtained for parameters of the *in vivo* experiment with a low deposition rate 1×10^{-4} ML/s. The average chain length is controlled by concentration of the C defects. The dependence of the average chain length on the C defect concentration is in Fig. 9(b). It can be seen that an effect of postdeposition relaxation disappears with the increasing concentration.

E. Growth scenario

The simulations and analysis of results allow to suggest a scenario for the experimentally observed submonolayer growth and discuss a role of participating processes at RT.

Simulations of the postdeposition relaxation show that only a population of atoms detached from chains exists on the surface after the deposition. They nucleate as new chains or attach to other chains and the system moves toward the dynamical equilibrium. During the deposition, if the deposition flux is small enough with respect to detachment rate and surface mobility, the growth proceeds at thermal equilibrium and a postdeposition effect consists from thermal fluctuations only; the scaled chain length distribution function is monotonously decreasing. At sufficiently high deposition flux, the growth of chains due to the attachment of deposited atoms dominates and the effect of the detachment is suppressed. The growth becomes irreversible and the scaled distribution function has a monomodal form (at almost isotropic surface diffusion).

F. Comparison with an equilibrium model

The model of Tokar and Dryssé[11] for the equilibrium homogeneous growth can provide the only parameter, the nearest-neighbor interaction energy V_{NN}^{x}. It can be determined from the dependence of the average chain length on coverage [using Eq. (14) in Ref. 11]. In case of the equilibrium model growth characteristics are independent of a kinetic path. Our data from *in vivo* experiments at a rather low deposition rate may reflect a situation not too far from an equilibrium state, but the considered growth is heterogeneous. The data in Fig. 4(b) can be approximated by an exponential scaling function. The value $V_{\mathrm{NN}}^{x}=-0.17$ eV obtained from our experimental data for indium is similar to the pair-interaction energy determined in Ref. 11 for gallium (−0.192 eV).

Simulations of experimental data showed that the deposition rate is a crucial parameter for growing indium on Si(100) surface at RT and determines a transition between irreversible and reversible character of the growth. The measured growth characteristics depend on a process of postdeposition relaxation, which has to be included into the growth simulation. The monotonous character of the scaled chain length distribution function can be related to a mechanism of atom detachment from the chains. The deposition rate and substrate temperature can be used for controlling the competition between *kinetics* and *equilibrium*. The model formulated for simulations is too simplified to be used for explanation all experimentally observed details;[19] for example, a plateau in the average chain length dependence on coverage within 0.05 and 0.12 ML (see Fig. 2) obtained from two various *in vivo* measurements—but the model explains the most important features of the growth of indium on the surface Si(100)-2×1 at room temperature.

VI. CONCLUSIONS

STM technique was used for studying the growth of indium on the Si(100)-2×1 surface at low coverage and room temperature. Direct observation during the deposition, *in vivo* measurements, showed that the *C* defects act as nucleation centers for indium adatoms. The majority of the indium chain is pinned on one or both ends by a *C* defect that determines the average chain length for a given coverage. The *in vivo* observations further revealed the reversible character of the growth due to atom detachment from the chains. Statistical characteristics of the In layers (average chain length, average length of chains not terminated at *C* defects, dependence of average chain length on coverage, and scaled island-size distribution function) were obtained from the experiments of two types: the *in vivo* measurements and the standard *in situ* observations after the deposition of various coverages.

The atomistic model with the anisotropic diffusion which includes the presence of *C* defects on the surface as well as the detachment of atoms from the chain was developed. Both *in vivo* and *in situ* experiments were simulated using the KMC method. The simulations showed that the process of atom detachment can explain the monotonously decreasing shape of the scaled chain length distribution function. Free parameters of the model, activation energies for anisotropic surface diffusion, were determined by the comparison of experimental and simulated characteristics of the indium layers. The values obtained for the activation energies (see Table II) correspond to almost isotropic surface diffusion in contrary with anisotropic data reported for the same group metals Ga and Al earlier.

ACKNOWLEDGMENTS

This work is a part of the research plan MSM 0021620834 that is financed by the Ministry of Education of the Czech Republic and was partly supported by Project No. 202/06/0049 of GACR, Project No. AV0Z 10100520 of ASCR, Project No. 227/2006/B of GAUK, Project No. 225/2006/B of GAUK, and Project No. 100907 of GAUK. The access to the METACentrum computing facilities provided under the research intent MSM 6383917201 is highly appreciated.

APPENDIX

The deviations between experimental and simulated characteristics were determined as follows: (i) for the average chain length $\langle s\rangle$,

$$D_i=(\langle s\rangle_{\mathrm{simulated}}-\langle s\rangle_{\mathrm{experiment}})^2, \tag{2}$$

(ii) for the dependence of average length on coverage,

$$D_{ii}=\sum_{\Theta=0.025\ \mathrm{ML}}^{\Theta=0.25\ \mathrm{ML}}\frac{1}{\sigma_{\Theta}^{2}}(\langle s\rangle_{\Theta}^{\mathrm{simulated}}-\langle s\rangle s_{\Theta}^{\mathrm{experiment}})^2, \tag{3}$$

where σ_{Θ}^{2} is a weight parameter—mean-square deviation of chain length at a given coverage Θ obtained from simulation experiments;

(iii) for the scaled chain length distribution functions,

$$D_{iii}=\sum_{s=1}^{s=\infty}(f_s^{\mathrm{simulated}}-f_s^{\mathrm{experiment}})^2, \tag{4}$$

where function values f_s are calculated for each chain length of s atoms contained in the data.

*ivan.ostadal@mff.cuni.cz

[1] J. Nogami, A. A. Baski, and C. F. Quate, Phys. Rev. B **44**, 1415 (1991).
[2] J. Nogami, S. Park, and C. F. Quate, Appl. Phys. Lett. **53**, 2086 (1988).
[3] A. A. Baski, J. Nogami, and C. F. Quate, Phys. Rev. B **43**, 9316 (1991).
[4] M. Kishida, A. A. Saranin, A. V. Zotov, V. G. Kotlyar, A. Nishida, Y. Murata, H. Okado, M. Katayama, and K. Oura, Appl. Surf. Sci. **237**, 110 (2004).
[5] B. Voigtländer and T. Weber, Phys. Rev. Lett. **77**, 3861 (1996).
[6] I. Ošt'ádal, P. Kocán, P. Sobotík, and J. Pudl, Phys. Rev. Lett. **95**, 146101 (2005).
[7] M. M. R. Evans and J. Nogami, Phys. Rev. B **59**, 7644 (1999).
[8] G. Brocks, P. J. Kelly, and R. Car, Phys. Rev. Lett. **70**, 2786 (1993).
[9] M. A. Albao, M. M. R. Evans, J. Nogami, D. Zorn, M. S. Gordon, and J. W. Evans, Phys. Rev. B **72**, 035426 (2005).
[10] P. Kocán, P. Sobotík, I. Ošt'ádal, J. Javorský, and M. Setvín, Surf. Sci. **601**, 4506 (2007).
[11] V. I. Tokar and H. Dreyssé, Phys. Rev. B **74**, 115414 (2006).
[12] N. Takeuchi, Phys. Rev. B **63**, 035311 (2000).
[13] R. J. Hamers and U. K. Köhler, J. Vac. Sci. Technol. A **7**, 2854 (1989).
[14] P. Kocán, P. Sobotík, and I. Ošt'ádal, Phys. Rev. B **74**, 037401 (2006).
[15] M. A. Albao, M. M. R. Evans, J. Nogami, D. Zorn, M. S. Gordon, and J. W. Evans, Phys. Rev. B **74**, 037402 (2006).
[16] P. Kocán, L. Jurczyszyn, P. Sobotík, and I. Ošt'ádal, Phys. Rev. B **77**, 113301 (2008).
[17] M. Z. Hossain, Y. Yamashita, K. Mukai, and J. Yoshinobu, Phys. Rev. B **67**, 153307 (2003).
[18] S. Okano and A. Oshiyama, Surf. Sci. **554**, 272 (2004).
[19] I. Ošt'ádal, J. Javorský, P. Kocán, P. Sobotík, and M. Setvín, J. Phys.: Conf. Ser. **100**, 072006 (2008).
[20] M. C. Bartelt and J. W. Evans, Phys. Rev. B **46**, 12675 (1992).
[21] C. Ratsch, A. Zangwill, P. Šmilauer, and D. D. Vvedensky, Phys. Rev. Lett. **72**, 3194 (1994).
[22] P. Sobotík and I. Ošt'ádal, Surf. Sci. **602**, 2835 (2008).
[23] M. Kotrla, Comput. Phys. Commun. **97**, 82 (1996).
[24] J. Evans and M. Bartelt, J. Vac. Sci. Technol. A **12**, 1800 (1994).